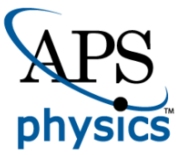

Beyond Chu's Limit with Floquet Impedance Matching

Huanan Li, Ahmed Mekawy, and Andrea Alù

Phys. Rev. Lett. **123**, 164102 — Published 16 October 2019

DOI: 10.1103/PhysRevLett.123.164102

Beyond Chu's Limit with Floquet Impedance Matching

Huanan Li[1], Ahmed Mekawy[1,2], and Andrea Alù[1,2,3,*]

[1]*Photonics Initiative, Advanced Science Research Center, City University of New York, New York, NY 10031, USA*

[2]*Department of Electrical Engineering, City College of The City University of New York, New York 10031, USA*

[3]*Physics Program, Graduate Center, City University of New York, New York, NY 10016, USA*

Chu's limit determines the minimum radiation quality factor Q of an electrically small resonator, and hence its maximum operational bandwidth, which is inversely proportional to its volume. This bound imposes severe restrictions in several areas of technology, from wireless communications to nanophotonics and metamaterials. Here, we show that a suitably tailored temporal modulation of the matching network, combined with proper detuning of the feeding impedance, can overcome this limit, and enable radiation over broader bandwidths, which scale as $1/\sqrt{Q}$ *, ensuring at the same time stability. Our findings open opportunities for communication systems, nanophotonics and sensor technology.*

Antenna minimization is of central importance in modern wireless communications due to the ever-increasing demand for compact versatile devices [1]. Electrically small antennas and resonators are crucial for portable wireless devices, medical equipment, sensors and communication systems, among several other applications. Chu's limit, originally derived over

*Corresponding author: aalu@gc.cuny.edu

seventy years ago [2], determines a minimum bound on the attainable radiation Q factor of small antennas, inversely proportional to their electrical volume, imposing severe constraints on their bandwidth of operation. Given the generality of this bound, which applies to any linear, passive, time-invariant open resonator, the efficiency-bandwidth product of small antennas is inherently limited and proportional to their volume [3]. This in turn implies a severe trade-off between the size of an antenna or a resonator and its bandwidth of operation.

To overcome Chu's limit, extensive research has been focused on active impedance matching techniques [4], using antenna loads that draw energy from amplifiers violating Foster's reactance theorem [5]-[9], see also [10]. Non-Foster antennas typically take advantage of negative-impedance converters to impedance match the antenna load over large bandwidths. However, they typically suffer from inherent instabilities and detrimental noise stemming from a combination of the active nature of the involved circuitry and its complexity and parasitics [11]. Recently, time-varying networks based on switched systems triggered when a pulse signal impinges on the load have been explored to overcome the bandwidth-size trade-off [12]-[15]. However, this approach requires synchronization of the incoming signals with the time variations in the matching network, and it is limited to pulsed operation.

In recent years, Floquet systems have been gaining increasing attention in the physics and engineering communities, highlighting how time modulation can empower systems with highly unusual properties overcoming limitations of passive time-invariant systems. Time modulation has been employed to enable Floquet topological phases [16]-[18], modulation-induced non-reciprocity [19]-[22], Floquet PT-symmetric systems [23]-[24], Floquet engineering [25]-[28] and scattering [29]-[30]. Here, we apply the exotic physics of temporally modulated systems to impedance matching, to overcome Chu's limit for signal transmission and gain in small antennas.

We prove that Floquet impedance matching can overcome the gain bandwidth vs. size trade-off of passive antenna systems, and it addresses the issue of instabilities and noise of non-Foster amplifier-based approaches. We validate our results within a realistic loop antenna loaded by a modulated varactor, and discuss the possible impact of these findings for other relevant technologies.

Electrically-small antennas and Chu's limit. — An antenna is electrically small if its electrical characteristic length $ka < 1/2$, where *k* is the wave number in free space and a is the radius of a sphere circumscribing it [4]. Small antennas are poor radiators, due to their high radiation quality factor $\mathrm{Q} = 2\omega_r \cdot \max\{W_E, W_M\}/P_{rad}$, where W_E/W_M is the time averaged stored electric/magnetic energy, P_{rad} is the radiated power and ω_r is the frequency of operation [2],[31]. In this definition, it is assumed that at ω_r the antenna is impedance matched, cancelling its large reactance via a matching network, and bringing it to resonance. Chu's limit determines a lower bound for the corresponding Q-factor: an electric dipole, for instance, has an approximate input impedance $Z_{in} \approx \eta\left(\frac{1}{jka} + (ka)^2\right)$ [2], characterized by a large reactance associated with the capacitance $C = \varepsilon_0 a$, and a small radiation resistance $R_r = \eta(ka)^2$, where ε_0 is the vacuum permittivity and η the impedance of free space (Fig. **1**). The quality factor $\mathrm{Q_{Chu}} = 1/(\omega_r R_r C) = 1/(k_r a)^3$, where $k_r = \omega_r/c_0$ (with c_0 being the speed of light in vacuum), increases inversely with the electrical volume $(k_r a)^3$, and thus becomes very large for small antennas. This value represents the minimum bound of the radiation Q-factor of a small antenna, known as Chu's limit [2],[3],[32]-[34]. Practical antennas can only yield a larger Q-factor by inducing additional stored energy within their physical structure. This in turn fundamentally limits the fractional bandwidth of operation, which is inversely proportional to Q.

Chu's limit is fundamentally rooted within the more general Bode-Fano bound on gain-bandwidth [35]-[37]. For passive, linear, time-invariant systems consisting of an antenna (e.g., a series resistance and capacitance) and the associated matching network (Fig. **1**), we have [38]

$$\int_0^\infty \frac{1}{\tilde{\omega}^2} \ln \frac{1}{\sqrt{1-T_0}} d\tilde{\omega} < \frac{\pi}{Q} \tag{1}$$

where the normalized (angular) frequency $\tilde{\omega} = \omega/\omega_r$, and the transducer gain T_0 is defined as the average power delivered to R_r over the maximum available average power at the source V_s. Eq. (1) is particularly restricting when matching an electrically small antenna, due to its high-Q nature. In this case, we necessarily expect a narrow gain peak around the operation frequency ω_r [4].

Floquet impedance matching —We establish a Floquet matching framework to go beyond the Bode-Fano bound for electrically small open resonators. For simplicity, we analyze the case of a small electric dipole antenna, impedance matched to the source through a time-modulated inductor $L(t) = L_0\big(1 + m\cos(\omega_M t)\big)$ [see Fig. **1**]. The static part L_0 is employed to compensate the antenna reactance and bring it to resonance at $\omega_r = 1/\sqrt{L_0 C}$. The modulation is introduced to impart parametric gain and overcome Chu's limit for passive networks, see also [39]-[40].

In order to evaluate the transducer gain $T_0(\omega)$ in this Floquet-matching circuit, and meanwhile study its stability, we construct the (normalized) Floquet scattering matrix $\overleftrightarrow{S}(s)$ in the complex excitation-frequency plane $\mathrm{s} = \sigma + j\omega, \omega \in (0, \omega_M)$. The Floquet $\overleftrightarrow{S}$-matrix, defined as $\vec{b} = \overleftrightarrow{S}\vec{a}$, connects the outgoing power wave amplitudes at different harmonics with the incoming ones [38], written collectively as output/input vectors $\vec{b}$ and $\vec{a}$:

$$\vec{a} \equiv \frac{1}{2\overleftrightarrow{k}}\left[\overleftrightarrow{y} \cdot \vec{V} + \vec{I}\right]; \quad \vec{b} \equiv \frac{1}{2\overleftrightarrow{k}_*}\left[\overleftrightarrow{y}_* \cdot \vec{V} - \vec{I}\right] \tag{2}$$

where the Floquet voltage $\vec{\mathrm{V}} = \begin{pmatrix} \vec{V}_1 \\ \vec{V}_2 \end{pmatrix}$ and current vectors $\vec{\mathrm{I}} = \begin{pmatrix} \vec{I}_1 \\ \vec{I}_2 \end{pmatrix}$ consist of the frequency-component of the voltages $\{v_1(t), v_2(t)\}$ and currents $\{i_1(t), i_2(t)\}$ as shown in Fig. **1**, e.g., $v_1(t) = \sum_n (\vec{V}_1)_n e^{s_n t} + c.c.$ with $s_n \equiv s + n \cdot j\omega_M$, etc.; the diagonal Floquet source admittance matrix $\overleftrightarrow{\mathrm{y}} = \begin{pmatrix} \overleftrightarrow{y}_1 & 0 \\ 0 & \overleftrightarrow{y}_2 \end{pmatrix}$ consists of two diagonal admittance submatrices $\overleftrightarrow{y}_1$ and $\overleftrightarrow{y}_2$, with diagonal entries $(\overleftrightarrow{y}_1)_{n,n} = 1/R_s$ and $(\overleftrightarrow{y}_2)_{n,n} = 1/\left(R_r + \frac{1}{Cs_n}\right)$ respectively; the diagonal matrix $\overleftrightarrow{k} = \begin{pmatrix} \overleftrightarrow{k}_1 & 0 \\ 0 & \overleftrightarrow{k}_2 \end{pmatrix}$ consists of two diagonal submatrices $\overleftrightarrow{k}_1$ and $\overleftrightarrow{k}_2$ with entries $\left(\overleftrightarrow{k}_1\right)_{n,n} = 1/\sqrt{R_s}$ and $\left(\overleftrightarrow{k}_2\right)_{n,n} = \frac{\sqrt{R_r}Cs_n}{R_r Cs_n + 1}$, and finally $\overleftrightarrow{k}_*(\{s_n\}) = \overleftrightarrow{k}^T(\{-s_n\})$ and $\overleftrightarrow{y}_*(\{s_n\}) = \overleftrightarrow{y}^T(\{-s_n\})$. The amplitude-squared of the matrix components $\overleftrightarrow{S}_{\alpha_r n_r, \alpha_c n_c}(j\omega)$ measures the average power delivered to port $\alpha_r = 1,2$ at frequency $\omega + n_r\omega_M, n_r \in \mathbb{Z}$, over the maximum available average power at the monochromatic source V_s of frequency $\omega + n_c\omega_M, n_c \in \mathbb{Z}$ and located at port $\alpha_c = 1,2$. Specifically, we have [41]

$$\overleftrightarrow{S} = -\overleftrightarrow{k}\overleftrightarrow{k}_*^{-1} + 2\overleftrightarrow{k}\left(\overleftrightarrow{y} + \overleftrightarrow{Y}\right)^{-1}\overleftrightarrow{k} \tag{3}$$

where the Floquet admittance matrix $\overleftrightarrow{Y}$ of the time-periodic matching inductor is $\overleftrightarrow{Y} = \begin{pmatrix} \overleftrightarrow{L}^{-1} & -\overleftrightarrow{L}^{-1} \\ -\overleftrightarrow{L}^{-1} & \overleftrightarrow{L}^{-1} \end{pmatrix}$ with submatrix $\overleftrightarrow{L}$ with components $\left(\overleftrightarrow{L}\right)_{n_r,n_c} = s_{n_r} L_{n_r - n_c}$, $L_n \equiv \frac{\omega_M}{2\pi}\int_0^{2\pi/\omega_M} L(t)e^{-jn\omega_M t}dt$.

We point out the structure similarity of Eq. (3) for the Floquet $\overleftrightarrow{S}$-matrix with a conventional coupled-mode formulation [22]. Hence, Eq. (3) enables an effective static-circuit description for the time-dependent scattering [29] under the high modulation-frequency expansion. This effective static circuit, resembling the concept of effective Hamiltonian for periodically driven quantum systems [25],[28], describes the response of the time-modulated circuit and allows defining the transducer gain $T_0(\omega) = \left|\overleftrightarrow{S}_{20,10}(j\omega)\right|^2$ in Eq. (1). In contrast to static circuits, $T_0(\omega)$ can go beyond the bound (1), because the system is time-varying and energy exchanges with the modulation network are allowed. Here, to calculate $T_0(\omega)$, we can directly work with the Floquet $\overleftrightarrow{S}$-matrix, or more conveniently, the Floquet transmission matrix $\overleftrightarrow{S}_{21}$ with input (output) at port 1 (port 2), a sub-block of $\overleftrightarrow{S}$, which reads

$$\overleftrightarrow{S}_{21} = 2\overleftrightarrow{k}_2\overleftrightarrow{y}_2^{-1}\left(\overleftrightarrow{L} + \overleftrightarrow{y}_2^{-1} + \overleftrightarrow{y}_1^{-1}\right)^{-1}\overleftrightarrow{y}_1^{-1}\overleftrightarrow{k}_1. \tag{4}$$

We can fully characterize the system using four dimensionless control parameters: two are driving-independent, the quality factor Q and the resistance ratio $\mathrm{r} = R_s/R_r$, the other two are driving-related, the relative modulation amplitude m and the normalized modulation frequency $\widetilde{\omega}_M = \omega_M/\omega_r$. Once the quality factor Q and operation frequency ω_r are specified, the parameters of the Chu-limited passive antenna, i.e., radiation resistance $R_r = \frac{\eta}{Q^{2/3}}$, capacitance $\mathrm{C} = \frac{1}{Q^{1/3}\omega_r\eta}$, size $a = \frac{c_0}{Q^{1/3}\omega_r}$ and static matching inductance $L_0 = \frac{\eta Q^{1/3}}{\omega_r}$, are determined. For example, if we choose $\mathrm{Q} = 100$ and $\omega_r = 2\pi \times 30\mathrm{MHz}$ in the radio-wave spectrum, we have $R_r \approx 17.5\Omega$, $\mathrm{C} \approx 3\mathrm{pF}$, $\mathrm{a} \approx 34$ cm and $L_0 \approx 9.3\mu\mathrm{H}$.

The temporal modulation of the matching network makes the system non-conservative at the operational frequency ω_r, and parametric gain can be used to reduce the numerator of Q (the

so-called "Q-energy" [31]), hence improving the bandwidth for fixed antenna size. We realize parametric gain by choosing $\widetilde{\omega}_M = 2$, which couples ω_r with $-\omega_r$ [42]. Around ω_r, the response of the system is well-approximated by the two-mode truncation of $\overleftrightarrow{S}_{21}$ in Eq. (4), yielding

$$\overleftrightarrow{S}_{21}^{(2)} \approx 2\frac{\sqrt{r}}{Q}\begin{pmatrix} \tilde{s}_{-1} + \frac{1}{\tilde{s}_{-1}} + \frac{1+r}{Q} & \tilde{s}_{-1}\frac{1}{2}m \\ \tilde{s}_0\frac{1}{2}m & \tilde{s}_0 + \frac{1}{\tilde{s}_0} + \frac{1+r}{Q} \end{pmatrix}^{-1}, \tag{5}$$

where the normalized complex frequencies $\tilde{s}_n = s_n/\omega_r$, and the transducer gain $T_0(\omega) \approx \left|\overleftrightarrow{S}_{21}^{(2)}(2,2)\right|^2$ with the argument indicating the entry of the matrix.

Parametric phenomena, however, are inherently frequency selective, hence the achieved parametric gain through modulation is expectedly narrow in bandwidth, rather than enhancing it, and it commonly induces instabilities [43]. This is seen in Fig. **2**(a), where we plot the transducer gain versus frequency for different values of m for the same resistance ratio $r = 1$, which ensures maximum gain in the static scenario. Starting from $m = 0$ (red line), we increase the modulation amplitude and achieve enhanced gain beyond the limit of passive systems, but over a reduced bandwidth. Here, we chose $m = 0.02, 0.05$ as two relevant examples, with the inset showing the evolution of the peak of T_0 with respect to m, which can be derived analytically from Eq. (5), $\mathrm{Max}(T_0) = 1/\left(1 - \frac{1}{16}m^2Q^2\right)^2$. The realizable gain diverges for $m = 4/Q$, indicating the boundary after which the system becomes unstable for $r = 1$. A clear trade-off arises between maximum achievable gain and stability of the system.

The phase diagram reported in Fig. **2**(b) and the associated stability region is a critical consideration when analyzing the Floquet matching scenario, as we need to avoid instabilities

that often jeopardize the design of non-Foster matching networks in other approaches [6]. The key advantage here is that the dispersion of parametric gain is carefully controlled through the modulation parameters. For each driving amplitude m, the instability threshold value r_{th} for the resistance ratio is determined solving σ_{pole}=Re$\left(s_{pole}\right) = 0$ for the first pole of the Floquet scattering matrix $\overleftrightarrow{S}$ in Eq. (**3**). Driving-affected poles can be obtained from $\det\left(\overleftrightarrow{y} + \overleftrightarrow{Y}\right) = 0$ in Eq. (**3**), leading to $\det\left(\overleftrightarrow{L} + \overleftrightarrow{y}_2^{-1} + \overleftrightarrow{y}_1^{-1}\right) = 0$. Under the two-mode approximation used to derive Eq. (**5**), we get $\widetilde{\omega}_{th}$=Im$\left(s_{pole}\right) = 1$ and $r_{th} = \frac{1}{2}mQ - 1$. Moreover, $\left.\frac{\partial\sigma}{\partial r}\right|_{\sigma=0} = -\frac{1}{2Q} < 0$, which ensures that the poles move away from the unstable half s-plane Re$(s) > 0$ when the resistance ratio further increases from $r = r_{th}$. Therefore, $r > r_{th} = \frac{1}{2}mQ - 1$ ensures stability for given m and Q. The inset of Fig. 2(a) and Fig. 2(b) explicitly show with different markers the location of the three gain curves in Fig. 2(a) for the considered values of m.

An available degree of freedom to ensure stability of our Floquet matching network is to control the source impedance in order to purposely introduce an impedance mismatch, and hence reduce the peak of the transducer gain. Impedance detuning acts as a form of negative feedback in the system, reducing the peak gain and proportionally enlarging the bandwidth of operation. We proceed to verify this prediction by choosing the resistance ratio $r_1 = R_s/R_r$ for each modulation amplitude m, so that $\max\left(T_0(\omega_r)\right) = 1$, i.e., a peak gain equal to the maximum in the non-modulated scenario. Fig. 2(b) shows the evolution of $r_1(m)$, which consistently lies in the stable region of the phase diagram. Controlling the source resistance can be obtained with a multisection transformer [41], and it is not bandwidth limited because there is no reactance involved, consistent with Eq. (1). Using Eq. (5), we find an explicit equation for $r_1(m)$:

$$(1+r_1)(1+r_1-2\sqrt{r_1}) = \frac{1}{4}m^2Q^2, \tag{6}$$

which determines a unique real-valued function $r_1(m) > r_{th}$ lying in the stable portion of Fig.**2**(b). As expected, from Eq. (6), $r_1 = 1$ when $m = 0$ produces the (static) impedance matching condition. In addition, $r_1(m) \propto m$ when mQ becomes large.

By employing Eqs. (5) and (6) and considering $\widetilde{\omega} \equiv \omega/\omega_r \approx 1$, we obtain the transducer gain dispersion $T_0(\omega)$ explicitly:

$$T_0(\omega) \approx \frac{1}{1+4(\widetilde{\omega}-1)^2\frac{Q^2}{r_1}\left(1-\frac{\sqrt{r_1}}{1+r_1}\right)^2} \tag{7}$$

indicating that the bandwidth B_T (in unit of ω_r), i.e., the full-width at half-maximum (FWHM), of the transducer-gain $T_0(\omega)$ in this optimal scenario is $B_T = \sqrt{r_1}/\left[Q\left(1-\frac{\sqrt{r_1}}{1+r_1}\right)\right] \to \sqrt{m/(2Q)}$ in the large mQ limit, much larger than $B_T \propto 1/Q$ in the static scenario [44]. Interestingly, the bandwidth of our stable Floquet matching network scales with $Q^{-1/2}$, ensuring significant broadening for electrically small antennas.

In Fig. **3**, we numerically illustrate the response of the active Floquet matching network, and the realistic opportunity of breaking Chu's limit in electrically small antennas based on this principle. Also here $\mathrm{Q} = 100$, corresponding to $k_r a \approx 0.215$. As m grows, the bandwidth of $T_0(\omega)$ increases considerably compared to the passive matching scenario when $m = 0$ [Fig. **3**(a)]. The theoretical curve is derived from Eq. (7) with $r = r_1(m)$ given from Eq. (6). In reality, the transmission line supporting the incoming waves from the source, has a fixed impedance R_t.

Therefore, as a further confirmation, we demonstrate bandwidth enhancement as seen in Fig. **3**(a) by incorporating an additional multisection transformer as part of the matching network, which is used to tune the Thevenin equivalent source resistance R_s as required for our purpose [41]. To see clearly the breaking of the Chu's limit, we show a direct comparison with the Bode-Fano bound in Eq. (1), see Fig. **3**(b). When $m = 0$, the passive matching is close to the Bode-Fano bound, as expected for highly reactive loads, and the system is above the Chu limit on the Q-factor [1]. As the modulation amplitude *m* increases, we go well beyond the Bode-Fano bound, without sacrificing transducer gain nor stability. Finally, we explore possible intermodulation distortions, which may be caused by the normalized transmittance $T_{-1}(\omega)$ at sideband $n = -1$ with frequency $\omega_{-1} = \omega - j\omega_M$. In this case, $T_{-1}(\omega) \approx \left|\overleftrightarrow{S}_{21}^{(2)}(1,2)\right|^2$ and we have

$$T_{-1}(\omega) \approx \left(1 - \frac{2\sqrt{r_1}}{1+r_1}\right)\frac{1}{1+4\frac{Q^2}{r_1}(\tilde{\omega}-1)^2}. \tag{8}$$

Under the positive frequency convention, this major sideband $|\omega_{-1}|$ sits symmetrically on the other side of the design frequency ω_r since $\omega_M = 2\omega_r$. Its peak value, i.e., $\max\{T_{-1}(\omega)\} = \left(1 - \frac{2\sqrt{r_1}}{1+r_1}\right)$, is smaller than the one of the transducer gain $T_0(\omega)$ in Eq. (7). In other words, the power transfer efficiency to the load at the same frequency is larger than any other harmonic.

*Realistic Implementation in a Loop Antenna Configuratio*n — To validate our results, we explore a realistic implementation in a loop antenna geometry [Fig. **4**(a)]. We simulated this geometry with CST Microwave Studio [45]. In Ref. [41], we characterize this realistic setup and demonstrate its inherent stability via time-domain simulations. In Fig. **4**(b), the dispersion of the transducer gain is compared with the one of a passive matching load, realized by a lumped series capacitance C_0 and a shunt inductance following an L-matching network. The antenna bandwidth

B_T is 11.3 MHz in contrast with 2.7MHz for passive matching. For loop antennas characterized by series inductance and resistance, the Bode-Fano Integral in Eq. (1) is modified to $\int_0^\infty \ln \frac{1}{\sqrt{1-T_0}} d\tilde{\omega}$ [38], which in our result yields a value of 0.06, which is beyond $\pi/Q_{\text{Chu}} \approx 0.03$ and thus confirms operation well beyond Chu's fundamental limit, see also Fig. **4**(b). Our Floquet matching network is therefore able to dramatically enhance the bandwidth performance compared to the passive scenario.

Conclusion—In this work, we discussed the concept of Floquet matching to broaden the gain bandwidth in electrically-small open resonators. A modulated matching network providing parametric gain, combined with suitable detuning of the source impedance, ensures bandwidth broadening for the transmitted signal, combined with inherent stability, without sacrificing the transducer peak gain. Our theory shows that the performance of the small antenna (i.e., gain-bandwidth product) increases proportional to $1/\sqrt{Q}$. We have validated our results in a loop antenna setup, including realistic parasitics. Similar concepts may be extended to time-varying nanophotonic circuit elements, with opportunities to broaden the resonant bandwidth in a variety of contexts, from sensing and nonlinearity enhancement, to metamaterial functionalities [46] and quantum photonics. In this scheme, the overall efficiency of the system is still limited, since a portion of the additional energy fed by the modulation network is routed back towards the source instead of being transmitted. Unwanted back reflections may be filtered out with non-reciprocal elements in the matching network, which may be again implemented using time modulation [20],[47]. More generally, we envision using multiple modulated matching elements with suitably tailored phases to combine parametric gain with gauge-field-like bias, which may route

the modulation network energy preferentially towards the antenna load, further enhancing the performance of Floquet matching networks.

Acknowledgements — This work was supported by the Air Force Office of Scientific Research and the Defense Advanced Research Projects Agency.

References

[1] J. L. Volakis, C-C Chen and K Fujimoto, *Small Antennas: Miniaturization Techniques & Applications* (McGraw-Hill, New York, 2010).

[2] L. J. Chu, "Physical limitations on omni-directional antennas," J. Appl. Phys. **19**, 1163 (1948).

[3] R. F. Harrington, "Effect of antenna size on gain, bandwidth and efficiency," J. Res. Nat. Bureau Stand., **64D**, 1 (1960).

[4] S. E. Sussman-Fort and R. M. Rudish, "Non-Foster Impedance Matching of Electrically Small Antennas," IEEE Trans. Antennas Propag. **57**, 2230 (2009).

[5] S. Hrabar, I. Krois, I. Bonic, and A. Kiricenko, "Negative capacitor paves the way to ultra-broadband metamaterials," Appl. Phys. Lett. **99**, 254103 (2011).

[6] E. Ugarte-Munoz, S. Hrabar, D. Segovia-Vargas, and A. Kiricenko, "Stability of Non-Foster Reactive Elements for Use in Active Metamaterials and Antennas," IEEE Trans. Antennas Propagat. **60**, 3490 (2012).

[7] N. Zhu, and R. W. Ziolkowski, "Design and measurements of an electrically small, broad bandwidth, non-Foster circuit-augmented protractor antenna," Appl. Phys. Lett. **101**, 024107 (2012).

[8] H. Mirzaei and G. V. Elefteriades, “A wideband metamaterial-inspired compact antenna using embedded non-Foster matching,” in *IEEE Antennas Propag. Soc. Int. Symp*., 1950 (2011).

[9] J. Church, J.-C. S. Chieh, L. Xu, J. D. Rockway, and D. Arceo, “UHF electrically small box cage loop antenna with an embedded non-Foster load,” IEEE Antennas Wireless Propag. Lett., **13**, 1329 (2014).

[10] K. Connor, “Chu’s limit—a limit no more,” *https://phys.org/news/2017-02-chu-limita-limit.html*, (2017).

[11] S. D. Stearns, “Incorrect stability criteria for non-Foster circuits,” in *Proceedings of Antennas and Propagation Society International Symposium (APSURSI), IEEE*, 2012.

[12] M. I. Jacob and H. N. Brauch, “Keying VLF transmitters at high speed,” Electronics, **27**, 148, (1954).

[13] M. Manteghi, "Fundamental Limits, Bandwidth, and Information Rate of Electrically Small Antennas: Increasing the Throughput of an Antenna Without Violating the Thermodynamic Q-Factor," IEEE Antennas and Propagation Magazine, **61**, 14 (2019).

[14] W. Yao, Y. E. Wang, "Direct antenna modulation - a promise for ultra-wideband (UWB) transmitting", Microwave Symposium Digest 2004, June 2004.

[15] A. Shlivinski and Y. Hadad, “Beyond the Bode-Fano Bound: Wideband Impedance Matching for Short Pulses Using Temporal Switching of Transmission-Line Parameters”, Phys. Rev. Lett. **121**, 204301 (2018).

[16] P. Titum, E. Berg, M. S. Rudner, G. Refael, and N. H. Lindner, “Anomalous Floquet-Anderson Insulator as a Nonadiabatic Quantized Charge Pump,” Phys. Rev. X **6**, 021013 (2016).

[17] R. W. Bomantara, G. N. Raghava, L. Zhou, and J. Gong, "Floquet topological semimetal phases of an extended kicked Harper model," Phys. Rev. E **93**, 022209 (2016).

[18] R. Fleury, A. B. Khanikaev and A. Alù, "Floquet topological insulators for sound," Nat. Commun. **7**, 11744 (2016).

[19] Z. Yu and S. Fan, "Complete optical isolation created by indirect interband photonic transitions," Nat. Photon. **3**, 91 (2009).

[20] N. A. Estep, D. L. Sounas, J. Soric, and A. Alù, "Magnetic-free non-reciprocity and isolation based on parametrically modulated coupled-resonator loops," Nat. Phys. **10**, 923 (2014).

[21] S. Taravati and C. Caloz, "Mixer-duplexer-antenna leaky-wave system based on periodic space-time modulation," IEEE Trans. Antennas Propag. **65**, 442 (2017).

[22] H. Li, T. Kottos, and B. Shapiro, "Floquet-network theory of nonreciprocal transport", Phys. Rev. Appl. **9**, 044031 (2018).

[23] M. Chitsazi, H. Li, F.□M. Ellis, and T. Kottos, "Experimental Realization of Floquet PT-Symmetric Systems,", Phys. Rev. Lett. **119**, 093901 (2017).

[24] T. T. Koutserimpas, A. Alù, and R. Fleury, "Parametric amplification and bidirectional invisibility in PT-symmetric time-Floquet systems", Phys. Rev. A **97**, 013839 (2018).

[25] N. Goldman and J. Dalibard, "Periodically Driven Quantum Systems: Effective Hamiltonians and Engineered Gauge Fields," Phys. Rev. X **4**, 031027 (2014).

[26] M. Bukov, L. D'Alessio, and A. Polkovnikov, "Universal High-Frequency Behavior of Periodically Driven Systems: from Dynamical Stabilization to Floquet Engineering," Adv. Phys. **64**, 139 (2015).

[27] A. Eckardt and E. Anisimovas, "High-frequency approximation for periodically driven quantum systems from a Floquet-space perspective," New J. Phys. **17**, 093039 (2015).

[28] A. Eckardt, Colloquium: Atomic quantum gases in periodically driven optical lattices, Rev. Mod. Phys. **89**, 011004 (2017).

[29] H. Li, B. Shapiro, and T. Kottos, "Floquet scattering theory based on effective Hamiltonians of driven systems," Phys. Rev. B **98**, 121101(R) (2018).

[30] H. Li and T. Kottos, "Design algorithms of driving-induced nonreciprocal components," Phys. Rev. Applied **11**, 034017 (2019).

[31] A. D. Yaghjian, "Overcoming the Chu lower bound on antenna Q with highly dispersive lossy material," IET Microw., Antennas Propag., **12**, 459 (2018).

[32] J. S. McLean, "A Re-Examination of the Fundamental Limits on the Radiation Q of Electrically Small Antennas," IEEE Trans. Antennas Propag. **44**, 672 (1996).

[33] D. M. Grimes and C. A. Grimes, "Minimum Q of Electrically Small Antennas: A Critical Review," Microwave Opt. Technol. Lett. **28**, 172 (2001).

[34] A. D. Yaghjian, M. Gustafsson, and L. Jonsson, "Minimum Q for lossy and lossless electrically small dipole antennas," Progr. Electromagn. Res., **143**, 641, (2013).

[35] H. W. Bode, *Network Analysis and Feedback Amplifier Design* (Van Nostrand, New York, 1945).

[36] R. M. Fano, "Theoretical limitations on the broadband matching of arbitrary impedances," J. Franklin Inst. **249**, 139 (1950).

[37] D. C. Youla, "A new theory of broadband matching," IEEE Trans. Circuit Theory **CT-11**, 30 (1964).

[38] D. M. Pozar, *Microwave Engineering* (Wiley, New York, 1998).

[39] M. Manteghi, “Antenna miniaturization beyond the fundamental limits using impedance modulation,” in Proc. IEEE Antennas Propag. Soc. Int. Symp. (2009).

[40] P. Loghmannia and M. Manteghi, “A Parametric Amplifier Slot Antenna,” *2018 IEEE International Symposium on Antennas and Propagation & USNC/URSI National Radio Science Meeting*, Boston, MA, 487, (2018).

[41] See Supplemental Material for further details.

[42] L. D. Landau and E. M. Lifshiftz, *Mechanics*, Vol. 1 (Course of Theoretical Physics) (Pergamon Press, 1976).

[43] K. M. Harish, B. J. Gallacher, J. S. Burdess and J. A. Neasham, “Experimental investigation of parametric and externally forced motion in resonant MEMS sensors,” J. Micromech. Microeng., **19**, 015021 (2009).

[44] A. D. Yaghjian and S. R. Best, “Impedance, bandwidth, and Q of Antennas,” IEEE Trans. Antennas Propag., **53**, 1298 (2005).

[45] https://www.cst.com.

[46] P. -Yen Chen, C. Argyropoulos, and A. Alù, “Broadening the Cloaking Bandwidth with Non-Foster Metasurfaces,” Phys. Rev. Lett., **111**, 233001 (2013).

[47] D. L. Sounas and A. Alù, “Non-reciprocal photonics based on time modulation,” Nat. Photon. **11**, 774 (2017).

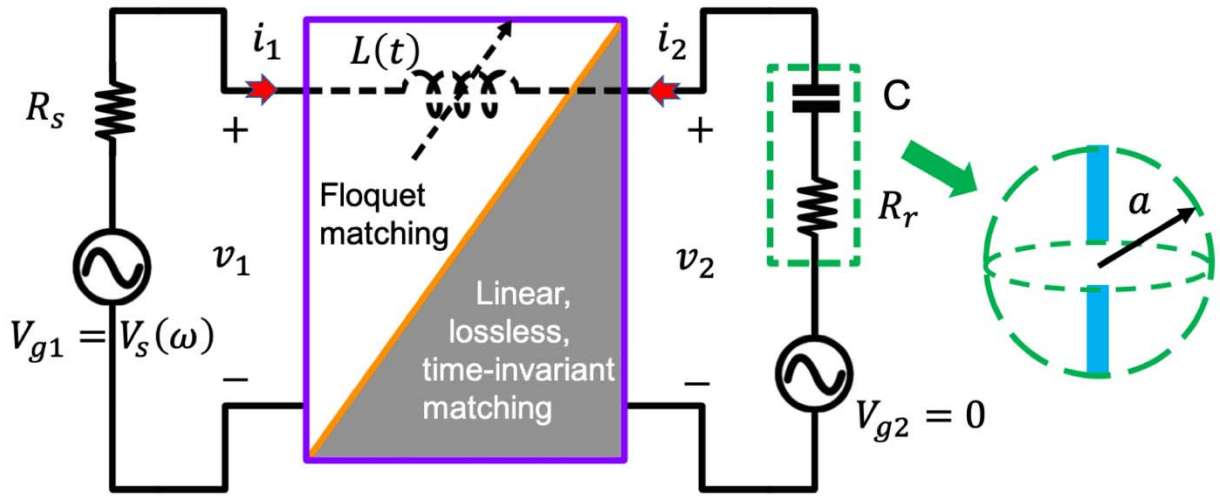

Fig. 1. Schematic of the Floquet matching network for an electric dipole, which is modeled as a series capacitance-resistance circuit. Floquet matching is achieved with a time-varying inductor (see dashed line).

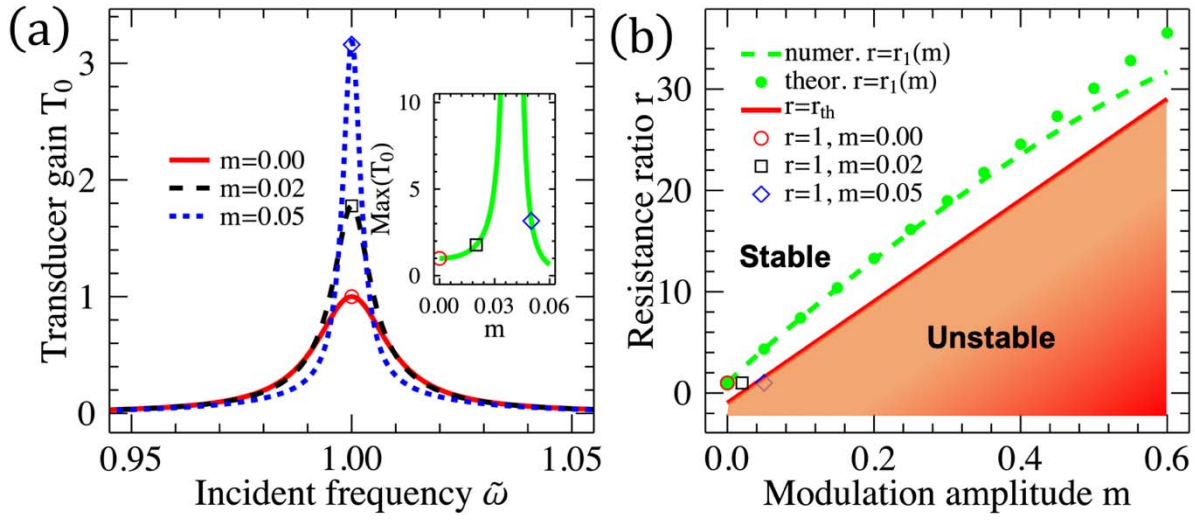

Fig. 2. (a) Transducer-gain as a function of the (normalized) excitation frequency of the source for (relative) modulation amplitude . In the inset, we show the maximum value of versus . (b) Stability phase diagram of the Floquet matching system in Fig. **1** in the

parameter space . Numerical (green dashed line) and theoretical (green circle) evolution of for . Here, , , and three typical scenarios for different are marked with different symbols.

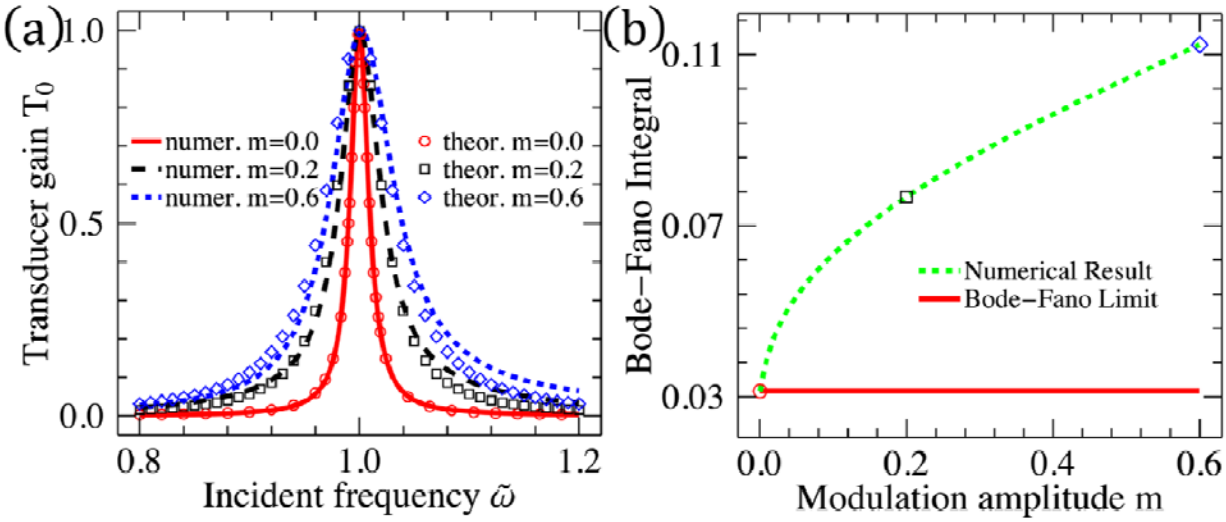

Fig. 3. Breaking Chu's limit using Floquet impedance matching with parametric gain. (a) transducer-gain versus (normalized) excitation frequency of the source, when the (relative) modulation amplitude . Numerical and theoretical results for are adopted from Fig. **2**(b). (b) Bode-Fano integral in Eq. (1) versus , showing operation beyond the Bode-Fano bound (red solid line). As increases, the resistance ratio is correspondingly tuned as . Other common parameters are the same as Fig. **2**.

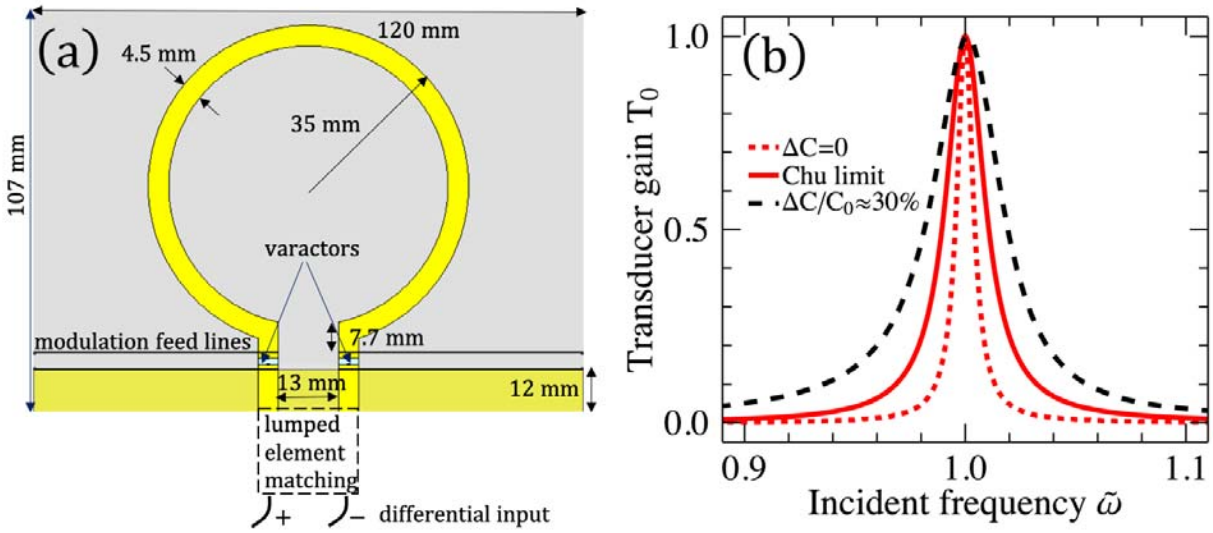

Fig. 4. Realistic simulation of Floquet matching of a loop antenna. (a) Geometry of a small loop antenna with electrical length at the design frequency , matched via a variable capacitor. The quality factor of the passive antenna is larger than Chu's limit . (b) Simulated transducer-gain as a function (black dashed line) of the normalized excitation frequency of the source, significantly surpassing passive matching (red dashed line). As a reference, the result for an ideal Chu-limit antenna is also shown (red solid line).